Day-to-day variability of the semidiurnal tide in the F-region ionosphere during the January 2021 SSW from COSMIC-2 and ICON

J. Oberheide[1]

[1]Department of Physics and Astronomy, Clemson University, Clemson, SC, USA

Key Points:

- Day-to-day variability of the semidiurnal tide in the F-region plasma resolved for the first time.
- Strength of polar vortex impacts ionosphere in both hemispheres on a day-by-day basis.
- Stratospheric winds variation of < 10 m/s change ionospheric plasma tides by a factor of 2.

Corresponding author: Jens Oberheide, `joberhe@clemson.edu`

Abstract

The semidiurnal tidal spectrum in the F-region ionosphere obtained from hourly COSMIC-2 Global Ionospheric Specification data assimilation is greatly ($> 50\%$) enhanced during the January 2021 Sudden Stratospheric Warming (SSW). Moreover, the semidiurnal migrating tidal response in topside electron densities closely follows the day-to-day changes of the 10 hPa, 60°N zonal wind from MERRA-2 during the SSW. The response is similar in the northern and southern crests of the Equatorial Ionization Anomaly (EIA) but persists towards higher magnetic latitudes and the EIA trough. A slight phase shift towards earlier local times is consistent with theoretical expectations of an E-region dynamo driving and agrees with semidiurnal tidal diagnostics of MIGHTI/ICON zonal winds at 105 km. The COSMIC-2 data are the first data set to resolve the tidal weather of the ionosphere on a day-to-day basis and, therefore, provide a new perspective on space weather variability driven by lower and middle atmosphere dynamics.

Plain Language Summary

Understanding the coupling between the weather of the troposphere and stratosphere with the space weather of the ionosphere has been one of the yet unsolved science challenges over the past decade. While progress has been made on seasonal and subseasonal timescales, the lack of sufficient global local time coverage data prevented further progress. The COSMIC-2 constellation now enables the community to make the next step and resolve global-scale ionospheric variability every hour. An unexpected finding is that even small wind changes (< 10 m/s) in the stratospheric polar vortex region are closely mapped into the global F-region, changing semidiurnal electron density amplitudes by almost a factor of two (peak-to-peak) within a few days.

1 Introduction

Much work has been done in the past decade to study the response of the low latitude ionosphere to Sudden Stratospheric Warmings (SSW), that is, a temporary breakup of the polar vortex in the stratosphere, which itself is a result of polar jet stream wobbles caused by Rossby waves. SSW related strato-/mesospheric wind and temperature changes cause a resonant amplification of the lunar semidiurnal migrating tide (M2, 12.42 hours) because of the atmospheric Pekeris mode (Forbes & Zhang, 2012), and a solar semidiurnal migrating tide (SW2, 12 hours) enhancement due to stationary planetary wave

interactions (e.g., Sathishkumar & Sridharan, 2013, and others) and changes in the ozone forcing of SW2 (e.g., Jin et al., 2012, and others). The pioneering work by Goncharenko et al. (2010) showed that these semidiurnal enhancements substantially modify the low latitude F-region ionosphere, mainly through tidally driven E-region dynamo changes with resulting mapping of polarization electric fields into the F-region and vertical plasma drifts. SSW also change the mean state of the thermosphere, i.e., in thermospheric composition. TIE-GCM simulations by Yamazaki and Richmond (2013) hypothesized that enhanced tides during SSW cause more wave breaking in the lower thermosphere, thus setting up an upward/poleward two-cell circulation in the lower thermosphere that depletes atomic oxygen. Molecular diffusion then propagates the depleted atomic oxygen throughout the whole thermosphere, causing a roughly 20% reduction of daytime mean O/N_2 column densities. This was recently confirmed by GOLD observations made during the 2019 SSW (Oberheide et al., 2020).

An outstanding science challenge in researching the SSW impact on the upper atmosphere is the lack of suitable global observations that allow one to resolve the tidal winds in the E-region dynamo on a daily basis, that is, the "tidal weather". Single satellite tidal wind diagnostics such as from TIDI/TIMED (Oberheide et al., 2011) or more recently MIGHTI/ICON (Forbes et al., 2022) can only resolve tidal variations on a monthly or longer timescale, similar to lunar tidal diagnostics from ICON and GOLD (Lieberman et al., 2022). Consequently, SSW variations, while still present, are considerably smoothed in MIGHTI/ICON tidal diagnostics. Data assimilation in the mesosphere/lower thermosphere, i.e., from systems like NAVGEM, can partly mitigate this challenge and provide realistic day-to-day tidal variations close to the E-region during SSW (Lieberman et al., 2015; Liu et al., 2022). Global-scale wave diagnostics in the ionosphere in response to SSW has been limited to planetary wave periods (e.g., Yamazaki et al., 2020, and others) due to the inherent limitations of single satellites or small constellations with insufficient local time resolution to diagnose the ionospheric tides on sub-monthly time scales.

This manuscript utilizes the new COSMIC-2 constellation to close this gap in our understanding of the ionospheric tidal response by utilizing hourly electron density profiles from the GIS data product. The target is the January 2021 SSW, characterized by 10 hPa, 60°N zonal winds that reversed between 5-Jan and 2-Feb with peak on 15-Jan and some intermittency. The semidiurnal tidal spectrum shows substantial day-to-day variations that are conclusively mapped to polar stratospheric wind variations with the

help of MIGHTI/ICON E-region tidal winds. The observed ionospheric tidal variations are unrelated to geomagnetic and solar variations. The results clearly show that even comparatively small wind variations in the polar vortex region have a large impact on the low latitude ionosphere, perhaps even more so than previously thought by the community and reported in the literature.

2 COSMIC-2 GIS Data and Tidal Diagnostics

The COSMIC-2 six satellite mission was launched on 25 June 2019 into a $\sim 24°$ inclination orbit. It provides in-situ electron density from the IVM instrument and thousands of daily RO soundings. The satellites are now in their final configuration near 530 km with a $\sim 60°$ longitude separation (Lin et al., 2020). GIS electron density is the hourly data product based on the Gauss-Markov Kalman filter (Lin et al., 2017), assimilating the ground-based Global Positioning System and space-based COSMIC-2 RO slant total electron content. GIS data are on $5° \times 2.5° \times 20$ km latitude/longitude/vertical grid, from pole-to-pole and 120 to 700 km.The results in Lin et al. (2020) and Rajesh et al. (2021) demonstrate the quality of the GIS electron density in the 200-500 km altitude range and their ability to resolve day-to-day tidal variability in the ionosphere.

For the ionospheric tidal diagnostics, the GIS data, which are provided in geographic coordinates, are first mapped into altitude adjusted geomagnetic coordinates (Shepherd, 2014). The tidal spectrum is then computed by 2-D Fourier fitting the GIS electron density at each altitude and magnetic latitude using one day of data, producing amplitudes and phases every day. The single day spectrum is exemplified in Figure 1, for January 6, 2021, 20°N magnetic latitude and 380 km. Apart from the mean and the diurnal signal moving westward with the relative motion of the Sun, a rich spectrum of tidal signals is observed, including the semidiurnal migrating tide (zonal wavenumber = -2) and several nonmigrating tides.

To minimize artifacts from solar and geomagnetic activity, the amplitudes are then normalized with the zonal mean daily mean (wavenumber 0, frequency 0) part of the Fourier fit at each latitude and altitude, that is, relative amplitudes in percent are provided with respect to the mean at given magnetic latitude and altitude. Figure 2a, b shows the time evolution of the semidiurnal part of the tidal spectrum over the 145 day period from DOY 279 (5-Oct 2020) to DOY 424 (27-Feb 2021) at 20°N and 20°S magnetic latitudes (EIA

crests) and 380 km, for zonal wavenumbers -6 (westward propagation) to +6 (eastward propagation). Note that the daily 2-D Fourier fitting of 1 hourly data does not allow one to separate between lunar (12.42 hours) and solar (12.0 hours) semidiurnal tides. The dominant semidiurnal migrating tide (zonal wavenumber -2) is enhanced between DOY 365 to DOY 410 in both hemispheres but with substantial variations within a few days. A similar behavior is observed throughout the bottomside and topside (Figure 2c, d). In the following, the focus will be on the semidiurnal migrating tide, as this component is large and, from a modeling point of view, very sensitive to SSW in the E-region dynamo (N. Pedatella et al., 2014).

E-region dynamo tidal winds are analyzed from MIGHTI/ICON day and nighttime observations of zonal winds below 110 km altitude, data version v04, which have been validated against meteor radars (Harding et al., 2021). As a single satellite, ICON only covers two local solar times (LST) a day. ICON is in a 27° inclination orbit that precesses 29.8 min/day towards earlier LST. Cullens et al. (2020) show that 35 days of data have to be combined into a composite day to obtain a LST coverage sufficient for tidal diagnostics at all latitudes (10°S to 40°N) observed by MIGHTI. The tidal diagnostics of the composite data is further explained in (Forbes et al., 2022) and follows the same procedure as for TIDI tidal winds (Oberheide et al., 2006). It is important to note that the E-region tides from MIGHTI shown in the next section 3 are running mean averages of 35-days of observation, in contrast to the "true" single data tides from COSMIC-2. Furthermore, the 35-day composite day approach for MIGHTI tides largely avoids "contamination" by the lunar semidiurnal tide: the latter is fully sampled in lunar local time over 9 consecutive days (Lieberman et al., 2022) such that the MIGHTI semidiurnal migrating tide is overwhelmingly from the solar part (SW2).

3 Discussion of SSW Response

The semidiurnal migrating tide SW2 response to the SSW in the E-region zonal wind is shown in Figure 3, as a function of geographic latitude and DOY, for amplitudes (panel a) and phases (panel b). Overplotted as a black line is the 10 hPa zonal mean zonal wind at 60°N as a measure for the SSW. The polar stratospheric zonal winds reversed (SSW) between 5-Jan and 2-Feb with peak on 15-Jan and some intermittency on the order of 10 m/s within a few days. The low latitude SW2 enhancement during the SSW is quite evident even in the 35-day running mean amplitudes, i.e., from less than 10 m/s

around DOY 340 to 30 m/s around DOY 375, at 20°N latitude. Tidal phases also shift by about 2-3 hours towards earlier times during the SSW. This is consistent with modeling expectations (N. Pedatella et al., 2014) of an SW2 phase shift during SSW.

The corresponding F-region plasma response is shown in Figure 4, as a function of magnetic latitude and DOY. An important difference is that the GIS data allow one to resolve the "true" day-to-day variations in the tides, while Figure 3 is a 35-day running mean. Three relevant findings emerge from the comparison with the polar stratospheric zonal winds that are again overplotted as a thick line (now in white). Firstly, the overall semidiurnal amplitudes in the plasma are enhanced by about 2-3 color scales (about 10-15 percent points, or by more than 50% SSW to non-SSW). Secondly, the phases slightly shift towards earlier times during the SSW, consistent with the observed neutral wind phase behavior in the E-region. Thirdly, and this is perhaps the most unexpected finding, there is a very close match between even small variations in the the polar stratospheric winds during the SSW and the F-region plasma response.

For example, the polar stratospheric wind change from -6.5 m/s on 6-Jan (DOY 372) to +2.6 m/s on 10-Jan (DOY 376) to -9.9 m/s on 15-Jan (DOY 381). The corresponding northern EIA crest amplitudes change from 45% to 25% to 45%. Similarly, the polar stratospheric winds are +16 m/s on 26-Jan (DOY 392), -1.3 m/s on 1-Feb (DOY 398), +19.6 m/s on 10-Feb (DOY 407), +15.2 m/s on 14-Feb (DOY 411), with corresponding northern EIA amplitudes of about 20%, 50%, 20%, 45%, respectively. As such, even small intermittencies in the polar stratospheric winds during SSW, a.k.a., the rather complex position and elongation of the polar stratospheric vortex plays a critical role in the day-to-day variability of the F-region plasma. It is important to note that this is not limited to the northern EIA crest but persists throughout all low and middle magnetic latitudes in both hemispheres and is similar in the bottomside F-region (compare Figure 2). The phases show a similar sensitivity: their day-to-day variability, while comparatively small, is nevertheless closely connected to the polar stratospheric vortex conditions. Solar and geomagnetic conditions do not play a role here as their day-to-day variability (Figure 4c) is very different to what is shown in Figure 4a, b.

The most likely mechanism to transmit the SSW signal into the plasma is certainly through E-region dynamo modifications, as initially proposed by Goncharenko et al. (2010). E-region dynamo modulation is also the most likely explanation for the close correspon-

dence between the day-to-day variations in the tidal wind and plasma amplitudes. N. M. Pedatella and Harvey (2022) recently reported a high correlation between the strength of the polar vortex and mesosphere/lower thermosphere tides from analyzing MLS data and SD-WACCMX model simulations, with a semidiurnal tidal reduction of about 25% during strong polar vortex times. Their modeled daily SW2 variability during northern hemisphere winter showed a linear correlation of -0.62 with daily variations in the strength of the polar vortex (expressed through the Northern Annular Mode). The COSMIC-2 observations in Figure 4 are consistent with this finding. Upward propagation meridional tidal winds and their day-to-day variability could play some role due to field-aligned plasma transport. But this question cannot be solved before day- and nighttime measurements can be made in the 110-200 km height region, to allow one to follow the height evolution of the semidiurnal tidal spectrum.

It is rather unlikely that thermospheric composition changes (as a source/sink of the plasma) play an important role in mapping the polar vortex strength variability into the F-region. The GOLD observations of the January 2019 SSW showed the importance of molecular diffusion for changing the upper thermospheric atomic oxygen (Oberheide et al., 2020), but the changes were on the order of 10% in 2019 (and 15% in 2021, not shown in this manuscript), which is too small to explain the SSW to non-SSW enhancement of 50%. Moreover, diffusion causes a time delay of a few days between dynamical changes in the lower thermosphere and the composition response in the upper thermosphere, and this is not evident in Figure 4.

4 Conclusions

The COSMIC-2 GIS data open a new window of opportunity to understand how weather-like variations from the lower atmosphere impact the global space weather of the ionosphere. The new capability to diagnose tides on a day-by-day basis shows a surprisingly close match with the strength of the polar vortex during SSW, consistent with very recent modeling studies that connected mesosphere/lower thermosphere semidiurnal tidal variability with daily variations in the Northern Annual Mode. Polar vortex wind changes on the order of 5-10 m/s during the January 2021 SSW cause relative electron density semidiurnal tidal amplitudes to change by a factor of two within a few days. The comparison with 35-day running mean tidal diagnostics from ICON supports E-region dynamo modulation as the leading coupling mechanism while thermospheric composi-

tion can be ruled out through previous diagnostics of GOLD data. The broader implications of the present work is that the shown day-to-day variability in the COSMIC-2 tides is not limited to SSW events but can potentially be expanded to non-SSW periods and connected to the dynamics of the troposphere and stratosphere that can be predicted several days or weeks in advance (like the Northern Annual Mode).

5 Open Research

COSMIC-2 GIS data are publicly available after free registration at `http://formosat7` `.earth.ncku.edu.tw/`. Conversion into geomagnetic coordinates was performed using the 20191229 release of the AACGM-v2 software from Dartmouth University, available at `http://superdarn.thayer.dartmouth.edu/aacgm.html`. MIGHTI/ICON v04 winds were obtained from `https://icon.ssl.berkeley.edu/Data/Data-Product-Matrix` and GOLD O/N$_2$ data were obtained from `https://gold.cs.ucf.edu/data/search/`. The 3-hourly K$_p$ index was obtained from GFZ Potsdam at `https://www.gfz-potsdam.de/` `en/kp-index/` website, the F10.7 cm radio flux from NASA/GSFC OMNIWeb at `https://` `omniweb.gsfc.nasa.gov/form/dx1.html` website, and the MERRA-2 stratospheric zonal mean zonal winds at 60°N and 10 hPa from NASA/GSFC Atmospheric Chemistry and Dynamics Laboratory at `https://acd-ext.gsfc.nasa.gov/Data_services/met/ann` `_data.html` website.

References

Cullens, C. Y., Immel, T. J., Triplett, C. C., Wu, Y.-J., England, S. L., Forbes, J. M., & Liu, G. (2020). Sensitivity study for ICON tidal analysis. *Progress in Earth and Planetary Science*, *7*(18). doi: 10.1186/s40645-020-00330-6

Forbes, J. M., Oberheide, J., Zhang, X., Cullens, C., Englert, C. R., Harding, B. J., ... Immel, T. J. (2022). Vertical Coupling by Solar Semidiurnal Tides in the Thermosphere From ICON/MIGHTI Measurements. *Journal of Geophysical Research: Space Physics*, *127*(5), e2022JA030288. Retrieved from `https://` `agupubs.onlinelibrary.wiley.com/doi/abs/10.1029/2022JA030288`

(e2022JA030288 2022JA030288) doi: https://doi.org/10.1029/2022JA030288

Forbes, J. M., & Zhang, X. (2012). Lunar tide amplification during the January 2009 stratosphere warming event: Observations and theory. *Journal of Geophysical Research: Space Physics*, *117*(A12). Retrieved from `https://agupubs.onlinelibrary.wiley.com/doi/abs/10.1029/2012JA017963` doi: 10.1029/2012JA017963

Goncharenko, L. P., Chau, J. L., Liu, H.-L., & Coster, A. J. (2010). Unexpected connections between the stratosphere and ionosphere. *Geophysical Research Letters*, *37*(10). Retrieved from `https://agupubs.onlinelibrary.wiley.com/doi/abs/10.1029/2010GL043125` doi: https://doi.org/10.1029/2010GL043125

Harding, B. J., Chau, J. L., He, M., Englert, C. R., Harlander, J. M., Marr, K. D., . . . Immel, T. J. (2021). Validation of ICON-MIGHTI Thermospheric Wind Observations: 2. Green-Line Comparisons to Specular Meteor Radars. *Journal of Geophysical Research: Space Physics*, *126*(3), e2020JA028947. Retrieved from `https://agupubs.onlinelibrary.wiley.com/doi/abs/10.1029/2020JA028947` (e2020JA028947 2020JA028947) doi: https://doi.org/10.1029/2020JA028947

Jin, H., Miyoshi, Y., Pancheva, D., Mukhtarov, P., Fujiwara, H., & Shinagawa, H. (2012). Response of migrating tides to the stratospheric sudden warming in 2009 and their effects on the ionosphere studied by a whole atmosphere-ionosphere model GAIA with COSMIC and TIMED/SABER observations. *Journal of Geophysical Research: Space Physics*, *117*(A10). Retrieved from `https://agupubs.onlinelibrary.wiley.com/doi/abs/10.1029/2012JA017650` doi: 10.1029/2012JA017650

Lieberman, R. S., Harding, B. J., Heelis, R. A., Pedatella, N. M., Forbes, J. M., & Oberheide, J. (2022). Atmospheric lunar tide in the low latitude thermosphere-ionosphere. *Geophysical Research Letters*, *49*(11), e2022GL098078. Retrieved from `https://agupubs.onlinelibrary.wiley.com/doi/abs/10.1029/2022GL098078` (e2022GL098078 2022GL098078) doi: https://doi.org/10.1029/2022GL098078

Lieberman, R. S., Riggin, D. M., Ortland, D. A., Oberheide, J., & Siskind, D. E. (2015). Global observations and modeling of nonmigrating diurnal tides

267   generated by tide-planetary wave interactions.   *Journal of Geophysical Re-*
268   *search: Atmospheres*, *120*(22), 11,419-11,437.   Retrieved from `https://`
269   `agupubs.onlinelibrary.wiley.com/doi/abs/10.1002/2015JD023739`   doi:
270   https://doi.org/10.1002/2015JD023739

271 Lin, C.-Y., Lin, C. C.-H., Liu, J.-Y., Rajesh, P. K., Matsuo, T., Chou, M.-Y., . . .
272   Yeh, W.-H.   (2020).   The Early Results and Validation of FORMOSAT-
273   7/COSMIC-2 Space Weather Products: Global Ionospheric Specification
274   and Ne-Aided Abel Electron Density Profile.   *Journal of Geophysical Re-*
275   *search: Space Physics*, *125*(10), e2020JA028028.   Retrieved from `https://`
276   `agupubs.onlinelibrary.wiley.com/doi/abs/10.1029/2020JA028028`
277   (e2020JA028028 2020JA028028) doi: https://doi.org/10.1029/2020JA028028

278 Lin, C. Y., Matsuo, T., Liu, J. Y., Lin, C. H., Huba, J. D., Tsai, H. F., & Chen,
279   C. Y.   (2017).   Data Assimilation of Ground-Based GPS and Radio Occul-
280   tation Total Electron Content for Global Ionospheric Specification.   *Journal*
281   *of Geophysical Research: Space Physics*, *122*(10), 10,876-10,886.   Retrieved
282   from `https://agupubs.onlinelibrary.wiley.com/doi/abs/10.1002/`
283   `2017JA024185`   doi: https://doi.org/10.1002/2017JA024185

284 Liu, G., Janches, D., Ma, J., Lieberman, R. S., Stober, G., Moffat-Griffin, T., . . .
285   Murphy, D. J.   (2022).   Mesosphere and Lower Thermosphere Winds and
286   Tidal Variations During the 2019 Antarctic Sudden Stratospheric Warming.
287   *Journal of Geophysical Research: Space Physics*, *127*(3), e2021JA030177.
288   Retrieved from `https://agupubs.onlinelibrary.wiley.com/doi/abs/`
289   `10.1029/2021JA030177`   (e2021JA030177 2021JA030177) doi: https://doi.org/
290   10.1029/2021JA030177

291 Oberheide, J., Forbes, J. M., Zhang, X., & Bruinsma, S. L.   (2011).   Climatology
292   of upward propagating diurnal and semidiurnal tides in the thermosphere.
293   *Journal of Geophysical Research: Space Physics*, *116*(A11).   Retrieved
294   from `https://agupubs.onlinelibrary.wiley.com/doi/abs/10.1029/`
295   `2011JA016784`   doi: 10.1029/2011JA016784

296 Oberheide, J., Pedatella, N. M., Gan, Q., Kumari, K., Burns, A. G., & Eastes,
297   R. W.   (2020).   Thermospheric Composition O/N_2 Response to an Altered
298   Meridional Mean Circulation During Sudden Stratospheric Warmings Ob-
299   served by GOLD.   *Geophysical Research Letters*, *47*(1), e2019GL086313.

Retrieved from https://agupubs.onlinelibrary.wiley.com/doi/abs/
10.1029/2019GL086313   (e2019GL086313 10.1029/2019GL086313)   doi:
https://doi.org/10.1029/2019GL086313

Oberheide, J., Wu, Q., Killeen, T. L., Hagan, M. E., & Roble, R. G.   (2006).
Diurnal nonmigrating tides from TIMED Doppler Interferometer wind
data: Monthly climatologies and seasonal variations.   *Journal of Geo-physical Research: Space Physics*, *111*(A10).   Retrieved from https://
agupubs.onlinelibrary.wiley.com/doi/abs/10.1029/2005JA011491   doi:
https://doi.org/10.1029/2005JA011491

Pedatella, N., Liu, H.-L., Sassi, F., Lei, J., Chau, J., & Zhang, X.   (2014).   Iono-sphere variability during the 2009 SSW: Influence of the lunar semidiurnal tide
and mechanisms producing electron density variability.   *Journal of Geophys-ical Research: Space Physics*, *119*(5), 3828-3843.   Retrieved from https://
agupubs.onlinelibrary.wiley.com/doi/abs/10.1002/2014JA019849   doi:
https://doi.org/10.1002/2014JA019849

Pedatella, N. M., & Harvey, V. L.   (2022).   Impact of Strong and Weak Strato-spheric Polar Vortices on the Mesosphere and Lower Thermosphere.   *Geophys-ical Research Letters*, *49*(10), e2022GL098877.   Retrieved from https://
agupubs.onlinelibrary.wiley.com/doi/abs/10.1029/2022GL098877
(e2022GL098877 2022GL098877) doi: https://doi.org/10.1029/2022GL098877

Rajesh, P. K., Lin, C. C. H., Lin, J.-T., Lin, C.-Y., Yue, J., Matsuo, T., . . . Chen,
C.-H.   (2021).   Day-to-day variability of ionospheric electron density during
solar minimum derived from FORMOSAT-7/COSMIC-2 measurements.   *Terr.
Atmos. Ocean. Sci.*, *32*, 1-17. doi: 10.3319/TAO.2021.08.01.01

Sathishkumar, S., & Sridharan, S.   (2013).   Lunar and solar tidal variabilities
in mesospheric winds and EEJ strength over Tirunelveli (8.7°N, 77.8°E)
during the 2009 major stratospheric warming.   *Journal of Geophysical
Research: Space Physics*, *118*(1), 533-541.   Retrieved from https://
agupubs.onlinelibrary.wiley.com/doi/abs/10.1029/2012JA018236   doi:
10.1029/2012JA018236

Shepherd, S. G. (2014). Altitude-adjusted corrected geomagnetic coordinates: Def-inition and functional approximations. *Journal of Geophysical Research: Space
Physics*, *119*(9), 7501-7521. Retrieved from https://agupubs.onlinelibrary

333   `.wiley.com/doi/abs/10.1002/2014JA020264`   doi: https://doi.org/10.1002/

334   2014JA020264

335 Yamazaki, Y., Matthias, V., Miyoshi, Y., Stolle, C., Siddiqui, T., Kervalishvili,

336   G., ... Alken, P.   (2020).   September 2019 Antarctic Sudden Stratospheric

337   Warming: Quasi-6-Day Wave Burst and Ionospheric Effects.   *Geophysi-*

338   *cal Research Letters*, *47*(1), e2019GL086577.   Retrieved from `https://`

339   `agupubs.onlinelibrary.wiley.com/doi/abs/10.1029/2019GL086577`

340   (e2019GL086577 10.1029/2019GL086577)   doi: https://doi.org/10.1029/

341   2019GL086577

342 Yamazaki, Y., & Richmond, A. D.   (2013).   A theory of ionospheric response to

343   upward-propagating tides: Electrodynamic effects and tidal mixing effects.

344   *Journal of Geophysical Research: Space Physics*, *118*(9), 5891-5905.   Retrieved

345   from `https://agupubs.onlinelibrary.wiley.com/doi/abs/10.1002/`

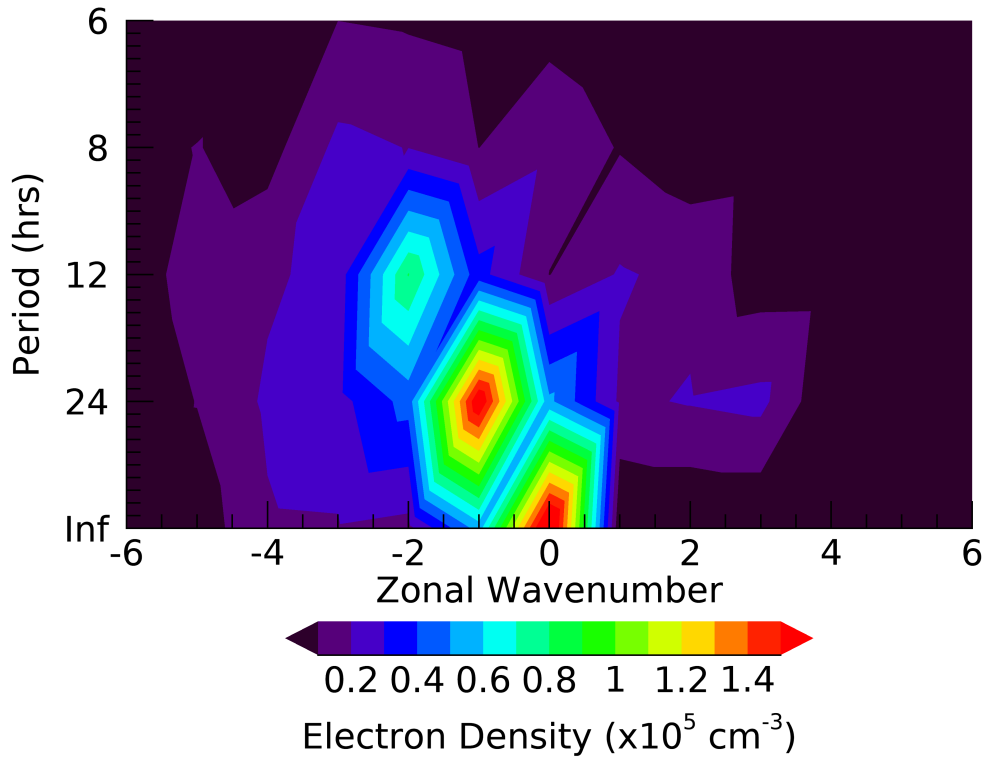346   `jgra.50487`   doi: 10.1002/jgra.50487

Figure 1. Tidal amplitude spectrum on January 6, 2021, at 380 km and 20°N magnetic latitude, from the COSMIC-2 GIS data set.
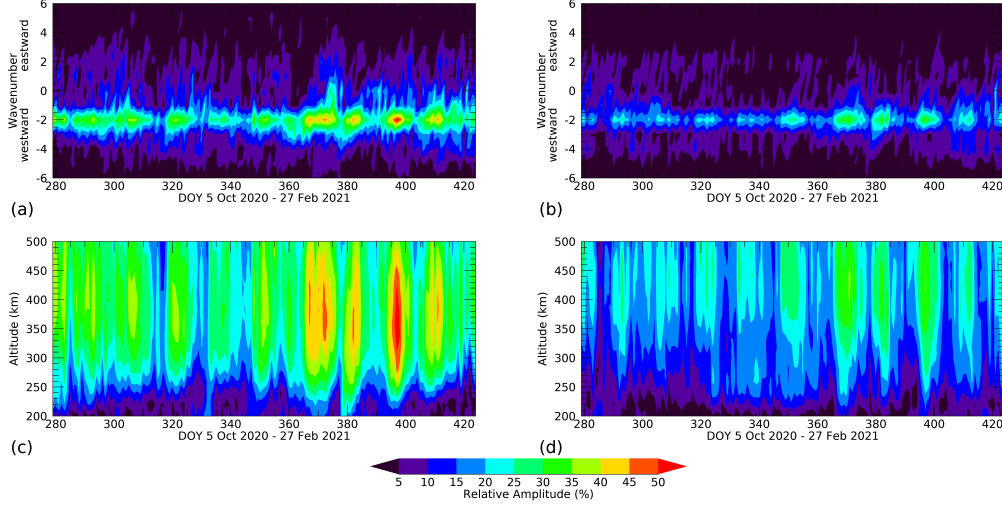
Figure 2. (a) Time evolution of the semidiurnal amplitude spectrum at 380 km and 20°N magnetic latitude. (b) Same as (a) but at 20°S magnetic latitude. (c) Semidiurnal migrating tide amplitude as function of time and altitude at 20°N magnetic latitude. (d) Same as (c) but for 20°S magnetic latitude. Plotted are relative amplitudes in percent, that is, relative to the zonal mean diurnal mean for each day, to remove geomagnetic variability effects.
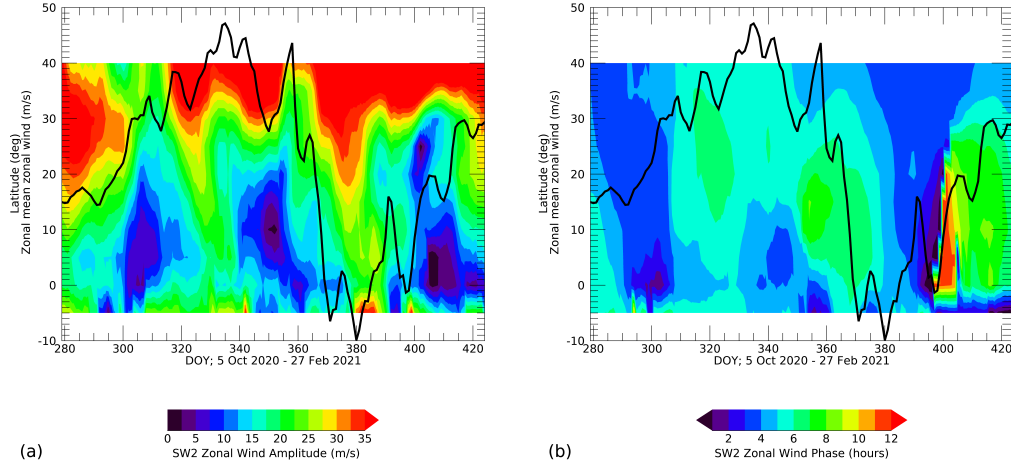

Figure 3. (a) Time evolution of the semidiurnal migrating tidal amplitudes in the zonal wind at 105 km from MIGHTI measurements. What is plotted are 35-day running means (±17 days around the day plotted) (b) Same as (a) but for tidal phases (universal time of maximum at 0° longitude). White areas indicate latitudes where tides cannot be derived from 35-day running mean composites. The black line in both panels is the zonal mean zonal wind at 10 hPa and 60°N from MERRA-2.
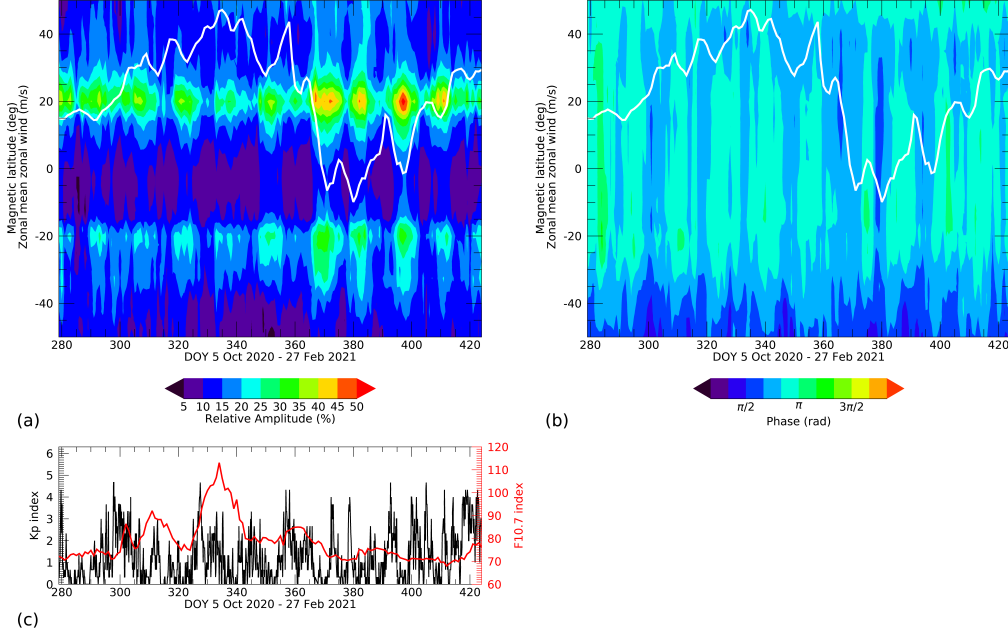
Figure 4. (a) Time evolution of the semidiurnal migrating tidal amplitudes from COSMIC-2 at 380 km as a function of magnetic latitude. (b) Same as (a) but for phases (rad of maximum). The white line in both panels is the zonal mean zonal wind at 10 hPa and 60°N from MERRA-2. Note the close correspondence of polar stratospheric winds and F-region electron density tides at all latitudes. (c) 3-hourly K_p index (black) and daily F10.7 index (red).